M&C 2017 - International Conference on Mathematics & Computational Methods Applied to Nuclear Science & Engineering, Jeju, Korea, April 16-20, 2017, on USB (2017)

A Reduced-Basis Element Method for Pin-by-Pin Reactor Core Calculations

Alexey L. Cherezov, Han G. Joo

Department of Nuclear Engineering, Seoul National University, 1 Gwanak-ro, Gwanak-gu, Seoul 08826, Korea
alcherezov.phd@gmail.com, joohan@snu.ac.kr

Abstract - *The reduced order model methods are very useful for real-time or many-query simulations of nuclear reactors. The common way for the reduced order models construction is a reduction of the preliminary calculated snapshots by the proper orthogonal decomposition methods. But an implementation of this approach for the high-fidelity real-size problems becomes very expensive due to a large computation cost of the one snapshot. To escape this problem the reduced basis element method is suggested to use. The method is based on a spatial decomposition of the reactor core and computation of the reduced bases on each subdomain. An efficiency of the method is confirmed by calculations of the two-dimensional core with pin-level resolution.*

I. INTRODUCTION

The recent trend in nuclear reactor analyses is the development of high-fidelity algorithms for multiphysics simulations with pin-level resolution. There are a few methods that are widely used for the high-fidelity simulation such as the method of characteristics (MOC), the Monte-Carlo (MC) method and the finite element method (FEM). These methods are very expensive even for a single state calculation. In many practical analyses, however, such high-fidelity simulations need to be performed repeatedly for safety analyses, control optimization and space-time diagnostics which require prohibitive computational costs. Therefore the reduction of the computing time keeping the accuracy is always desired.

One of the possible ways for such reduction apart from parallelization is to use the reduced order model (ROM) methods. These are the family of methods aiming at a reduction in the dimension of a complex model without significant losses in the accuracy of the results. These methods allow a real-time simulation or fast calculations of a various core states needed for design analyses.

Because the FEM allows an explicit approximation of the solution over all the phase space, it is one of the most convenient discretization methods for the reduction procedure employed in the ROM. In this regard, there has been strong mathematical background in the reduction algorithms based on FEM. This was named the reduced basis (RB) methods [1], [2].

The basic idea of the RB method is the construction of a reduced basis which has a small dimension by processing of high-fidelity snapshots. The reduced basis is determined using the proper orthogonal decomposition (POD) methods designed for the optimal approximation of given set of vectors or functions. These methods are often used in the different areas of nuclear reactor analyses and include the principal component analysis (PCA), singular-value decomposition (SVD) and Karhunen-Loeve decomposition (KLD) [3].

According to the RB method computations are split into two parts: an expensive off-line and inexpensive on-line phases. During the off-line phase a generation of snapshots, construction of reduced bases and assembling of ROM matrices are carried out. After that a fast evaluations of the solution is performed at the on-line phase. For the proper set of snapshots the ROM allows to reproduce the solutions with a sufficient accuracy. A high potential and practice utility of the RB method has been demonstrated by the works [4],[5].

The RB methods use the reduced bases determined on the whole spatial domain of the given problem. Therefore a large number of high-fidelity snapshots have to be calculated by the initial non-reduced order model. But there are a very large problems which solutions could not be calculated due to the memory or/and time constraints. Therefore an another approach is become necessary where the initial spatial domain is divided into an adequate small fragments. The reduced bases are calculated on each of them and then merged in all parts into a global interpolant defined on the initial domain. This approach is named Reduced Basis Elements (RBE) method and has been developed by [6].

The ROM produced by RBE method has a greater dimension compared with the one produced by RB method. Instead there is an advantage because the generation of snapshots requires a much less computation resources in RBE case. The main obstacle with the RBE method implementation is the need of proper boundary conditions at the fragments which are used during the snapshots calculations. At the present paper a simple approach is developed to get over this obstacle and then RBE method is applied for the pin-level reactor core steady-state problem.

II. METHODOLOGY

The RBE method could be explained trough the four steps which depicted on the diagram Fig.1. At the first step a given domain is split up into a set of non-overlapping subdomains forming a coarse mesh. It is obviously that the greater a dimension of the initial model the more efficient the reduction approach is. Therefore we will assume the coarse subdomains have a pin-level heterogeneous structure and a large number of degrees-of-freedom is required for an accurate representation of a neutron flux distribution inside. For example an assembly-wise map could be used for a coarse mesh partition. As a result all subdomains have the same rectangular or hexagonal form.

At the second step a neutron diffusion equation is solved for a given coarse subdomain with using an ordinary FEM. A fine mesh partition and polynomial basis functions are used

here. Because the boundary conditions are unknown the set of solutions or so called snapshots are calculated for different distributions of the incoming currents.

At the third step the snapshots are approximated by an optimal set of orthogonal functions using the PCA analysis. The obtained principal components are ranged by a contribution in the error of approximation. Then the first few of them form the basis of the reduced subspace which applied for the considered subdomain.

After all subdomains have been passed the last step is performed where the diffusion eigenvalue problem is solved on the given domain using the FEM method with the coarse mesh and prepared reduced basis functions are employed. Because the reduced bases are determined independently the basis functions could not be patched continuously at the surfaces of the adjacent subdomains. Therefore the Discontinuity Galerkin (DG) method is became necessary where the solution is sought in a space of discontinuity functions with discontinuity derivatives. In present work we will use the DG method which developed by [7] special the for diffusion equations.

1. Solution on the coarse mesh

Let us consider the M-group diffusion neutron balance equation in domain Ω:

$$-div\left(\hat{D}\nabla\boldsymbol{\phi}\right)+\hat{\Sigma}\boldsymbol{\phi}=\frac{1}{k_{ef}}\hat{F}\boldsymbol{\phi}, \tag{1}$$

with the boundary conditions $\boldsymbol{\phi}|_{x\in\Gamma_D}=0$. Here $\hat{D}$ is diagonal matrix of diffusion coefficients, $\hat{\Sigma}$ is a non-symmetric matrix which entries are an absorption and group transfer macroscopic cross-sections, $\hat{F}$ is a matrix of fission source, $\boldsymbol{\phi}=(\phi_1(x),...,\phi_M(x))^T$ is a vector of group-wise neutron fluxes and k_{ef} is a maximum eigenvalue.

Let us assume that the domain Ω can be decomposed into a non-overlapping union of subdomains Ω_i. The adjacent boundaries are the lines in 2D or planes in 3D case. The normal vector $\boldsymbol{n}$ on the common boundary Γ_{ij} between two adjacent subdomains Ω_i and Ω_j has the direction from one with greater index. The considered partition $P_K(\Omega)=\{\Omega_k, k=1,...,K\}$ we will call the coarse mesh on Ω.

Follow the FEM theory we need to introduce the Hilbert space $H^1(\Omega)$ of continuous vector functions with continuous derivatives on Ω. According to the mixed CG method the solution of the diffusion equation is approximated by a trial vector function $\boldsymbol{u}$ from this space. Let us denote $\nabla_{\boldsymbol{n}}\cdot=(\nabla\cdot,\boldsymbol{n})$ and $\langle\bullet\bullet\rangle_\Omega$, $\langle\bullet,\bullet\rangle_\Gamma$ are the scalar products with integrals over domain Ω and boundary Γ. Then the week formulation of the diffusion equation 1 in CG approach is

$$a_0(\boldsymbol{u},\boldsymbol{v})=\frac{1}{k_{ef}}b(\boldsymbol{u},\boldsymbol{v}), \tag{2}$$

where $\boldsymbol{u},\boldsymbol{v}\in H^1(\Omega)$ and bilinear forms are

$$a_0(\boldsymbol{u},\boldsymbol{v})=\left\langle\hat{D}\nabla\boldsymbol{u},\nabla\boldsymbol{v}\right\rangle_\Omega+\left\langle\hat{\Sigma}\boldsymbol{u},\boldsymbol{v}\right\rangle_\Omega+\left\langle\hat{D}\nabla_{\boldsymbol{n}}\boldsymbol{v},\boldsymbol{u}\right\rangle_{\Gamma_D}-\left\langle\hat{D}\nabla_{\boldsymbol{n}}\boldsymbol{u},\boldsymbol{v}\right\rangle_{\Gamma_D} \tag{3a}$$

$$b(\boldsymbol{u},\boldsymbol{v})=\left\langle\hat{F}\boldsymbol{u},\boldsymbol{v}\right\rangle_\Omega \tag{3b}$$

Now we need to formulate the weak form according to DG approach. We will take for that the broken space $H^1(P_K)$ which consists of the piece-wise continuous functions $\boldsymbol{f}$ defined on the whole domain Ω so that $\boldsymbol{f}\in H^1(\Omega_k)$ for $\Omega_k\in P_k(\Omega)$. Then a solution is approximated by a trial function $\boldsymbol{u}$ which from the space $H^1(P_K)$. As a result the neutron flux and current have the discontinuities on the boundaries Γ_{ij} and additional coupling terms have to established in the week formulation.

Follow the [7], [8] we define on Γ_{ij} the jump operator $[g]=(g^- - g^+)$ and average operator $\{g\}=(g^-+g^+)/2$ where functions g^+ and g^- are taken from the adjacent subdomains Ω_i and Ω_j accordingly if $i>j$. Let us introduce a new bilinear form

$$a(\boldsymbol{u},\boldsymbol{v})=a_0(\boldsymbol{u},\boldsymbol{v})+\left\langle\left\{\hat{D}\nabla_{\boldsymbol{n}}\boldsymbol{v}\right\},[\boldsymbol{u}]\right\rangle_{\Gamma_{int}}+\left\langle\left\{\hat{D}\nabla_n\boldsymbol{u}\right\},[\boldsymbol{v}]\right\rangle_{\Gamma_{int}}, \tag{4}$$

where Γ_{int} is a set of inter-element boundaries. Then the week formulation of the diffusion equation 1 according to DG approach is

$$a(\boldsymbol{u},\boldsymbol{v})=\frac{1}{k_{ef}}b(\boldsymbol{u},\boldsymbol{v}), \tag{5}$$

where $\boldsymbol{u},\boldsymbol{v}$ and $D\nabla_{\boldsymbol{n}}\boldsymbol{u}\in H^1(\Omega)$.

It is worth to note that considered method is applied right for the diffusion equation in the form 1. Therefore the transformation into a system of flux and current equations is not necessary unlike other DG schemes. Compared with CG scheme a number of unknowns are increased only by a presence of discontinuities across the interfaces.

The important advantage of the equation 5 is there are not Lagrange multipliers and unknown penalty parameters. The convergence of the scheme is $O(h^2)$ for second order polynomial approximation. The bilinear form $a(\boldsymbol{u},\boldsymbol{v})$ renders a positive define, well-conditioned matrix and standard iterative and acceleration methods could be used for solution.

2. Simulation of Boundary Conditions

In a previous section the solution have been approximated by the discontinuity functions from the broken space. Now we need to setup the appropriate basis functions on the subspaces $H^1(\Omega_k), \Omega_k\in P_k(\Omega)$. According to the RBE method the set of snapshots should be determined for this aim.

The considered coarse subdomains have a complex heterogeneous structure. Therefore incoming currents on the boundaries could not be approximated by the low order polynomials or other simple functions. For a proper simulation of the boundary conditions the patterns of adjacent subdomains should be considered rather then single subdomains.

In a simplest case we can split the coarse mesh up the non-overlapping patterns which consist of the 2×2 or $2\times2\times2$ subdomains for the 2D or 3D geometry. As a result we get a pool of patterns with all encountered combinations of subdomains. If a few types of subdomains are used only then there is a sense to group the patterns relatively a rotation and

reflection symmetry. By this way we can significantly reduce the size of the patterns pool.

There are a few ways how to generate the snapshots for the given pattern. For example we can get the solutions of an eigenvalue problem for the different albedo conditions on the boundaries. The snapshots are taken from the each subdomain of the pattern. In this case a lot of eigenvalue calculations are required. And if a size of the patterns pool is large the off-line phase of computations is became too expensive. Moreover it is not clear how to chose the suitable range of the albedo values which could be depend on a subdomain's type.

For these reasons an another approach is suggested to use. It is well-known that the low-order harmonics are converged very slowly during a power iterations unlike the high-order ones. This feature could be employed to replace the set of eigenvalue problems with the different albedo conditions by the one power iteration process. While going the process the snapshots are fetched right from the approximate solution arising on the regular iteration. An error of the solutions could be used for the rejection of too closed snapshots. It is worth to note that the slow convergence of power iterations the more various snapshots are generated. Therefore a shift acceleration method is suggested not to use.

Let us denote $\{\boldsymbol{u}_n, n = 1, ..., N\}$ the set of snapshots generated for the subdomain Ω_k. It is calculated by the CG method using a finite piece-wise polynomial subspace of the space $H^1(\Omega_k)$ where the basis $\{\chi_i, i = 1, ..., S\}$ is employed. Therefore the snapshots could be written in the form

$$\boldsymbol{u}_n = \sum_{i=1}^{S} z_{i,n}\boldsymbol{\chi}_i \quad \text{in} \quad \Omega_k, \tag{6}$$

and represented by the vector of coefficients $\boldsymbol{z}_n = (z_{1,n}, ..., z_{S,n})^T$.

3. Reduced Basis Functions

When the coefficients $\{\boldsymbol{z}_n, n = 1, ..., N\}$ have been determined the basis functions are calculated as follow. According to PCA analysis the covariance matrix

$$\hat{M} = (\boldsymbol{x}_1, ..., \boldsymbol{x}_N)^T(\boldsymbol{x}_1, ..., \boldsymbol{x}_N) \tag{7}$$

is assembled from the centered values $\boldsymbol{x}_n = \boldsymbol{z}_n - \boldsymbol{q}_0$, where $\boldsymbol{q}_0 = \frac{1}{N}\sum_{n=1}^{N} \boldsymbol{z}_n$ is an averaged vector.

Then the first S_r eigenvalues λ_i and eigenvectors $\boldsymbol{y}_i$ of the matrix $\hat{M}$ are calculated and ranged by the values of explained variance ratios:

$$\sigma_i = \frac{\lambda_i}{\lambda_1 + \lambda_2 + ... + \lambda_{S_r}}. \tag{8}$$

Because the averaged vector $\boldsymbol{q}_0$ is not orthogonal to principal components $\boldsymbol{y}_i$ then the Gramm-Schmidt orthogonalization process is applied for a set of vectors $\{\boldsymbol{q}_0, \boldsymbol{y}_1, ..., \boldsymbol{y}_{S_r}\}$ started with positive vector $\boldsymbol{q}_0$. The result is a set of orthogonal vectors $\{\boldsymbol{q}_0, \boldsymbol{q}_1, ..., \boldsymbol{q}_{S_r}\}$.

After all the truncated subspace employed for model reduction consists of the $S_r + 1$ basis functions

$$\boldsymbol{\psi}_{k,s} = \sum_{i=1}^{S} q_{s,i}\boldsymbol{\chi}_i \quad \text{in} \quad \Omega_k \quad \text{for} \quad s = 0, 1, ..., S_r, \tag{9}$$

and numerical solution according to RBE method is approximated as follow:

$$\boldsymbol{u}_{RBE} = \sum_{k=1}^{K}\sum_{s=0}^{S_r} c_{k,s}\boldsymbol{\psi}_{k,s} \quad \text{in} \quad \Omega. \tag{10}$$

4. Algebraic Formulation of RBE Method

For given sets of reduced bases the week form 5 is transformed into a left $\hat{L}$ and right $\hat{R}$ hand side block matrices. The dimension of matrices equals $K \times S_r$, where K is a number of coarse subdomains and S_r is a number of reduced basis functions. Unlike the right hand side matrix which has diagonal blocks $\hat{R}_{kk}$ only the left hand side matrix consists of the diagonal $\hat{L}_{kk}$ and non-diagonal $\hat{L}_{k,j}$ block-matrices both. The non-diagonal blocks corresponds to the coupling terms of a weak equation. The block matrices are assembled in two steps.

At first the large $(S \times S)$-matrices $\hat{A}_k, \hat{I}_{kk}, \hat{I}_{kj}$ and $\hat{B}_k$ are assembled in the subdomains Ω_k corresponding to the bilinear forms:

$$A_k(\boldsymbol{u}, \boldsymbol{v}) = \left\langle \hat{D}\nabla\boldsymbol{u}, \nabla\boldsymbol{v}\right\rangle_{\Omega_k} + \left\langle \hat{\Sigma}\boldsymbol{u}, \boldsymbol{v}\right\rangle_{\Omega_k} + \left\langle \hat{D}\nabla_{\boldsymbol{n}}\boldsymbol{v}, \boldsymbol{u}\right\rangle_{\Gamma_k^{bnd}} - \left\langle \hat{D}\nabla_{\boldsymbol{n}}\boldsymbol{u}, \boldsymbol{v}\right\rangle_{\Gamma_k^{bnd}}, \tag{11}$$

$$I_{kk}(\boldsymbol{u}, \boldsymbol{v}) = \frac{1}{2}\sum_{j\in J_k}\left(\left\langle \hat{D}^+\nabla_{\boldsymbol{n}}\boldsymbol{v}^+, \boldsymbol{u}^+\right\rangle_{\Gamma_k} - \left\langle \hat{D}^+\nabla_{\boldsymbol{n}}\boldsymbol{u}^+, \boldsymbol{v}^+\right\rangle_{\Gamma_k^{bnd}}\right), \tag{12}$$

$$I_{k,j}(\boldsymbol{u}, \boldsymbol{v}) = -\frac{1}{2}\left(\left\langle \hat{D}^+\nabla_{\boldsymbol{n}}\boldsymbol{v}^+, \boldsymbol{u}^-\right\rangle_{\Gamma_{k,j}} + \left\langle \hat{D}^+\nabla_{\boldsymbol{n}}\boldsymbol{u}^-, \boldsymbol{v}^+\right\rangle_{\Gamma_{k,j}}\right), \tag{13}$$

$$B_k(\boldsymbol{u}, \boldsymbol{v}) = \left\langle \hat{F}\boldsymbol{u}, \boldsymbol{v}\right\rangle_{\Omega_k}. \tag{14}$$

Here the functions $\boldsymbol{u}$ and $\boldsymbol{v}$ are elements of the basis $\boldsymbol{\chi}_{k,s}$. Because the snapshots and reduced basis functions are calculated in the same finite element basis then the reduction procedure for the large matrices could be applied:

$$\hat{L}_{kk} = \hat{Y}_k^T\left(\hat{A}_k + \hat{I}_{kk}\right)\hat{Y}_k, \tag{15}$$

$$\hat{L}_{kj} = \hat{Y}_k^T\hat{I}_{kj}\hat{Y}_j, \quad \text{for} \quad j \in J_k, \tag{16}$$

$$\hat{R}_{kk} = \hat{Y}_k^T\hat{B}_k\hat{Y}_k. \tag{17}$$

After all blocks are assembled the matrix eigenvalue problem is solved:

$$\hat{L}\boldsymbol{x} = \frac{1}{k_{ef}}\hat{R}\boldsymbol{x}, \tag{18}$$

where vector $\boldsymbol{x}$ consists of the neutron flux expansion coefficients in reduced subspace.

Thanks for the DG method the assembling and reduction of block matrices is performed for each coarse domain independently. That is very convenient for parallelization. The memory requirements are depend on the sizes of for matrices $\hat{L}$, $\hat{R}$ and preconditioners. Therefore the solution of the huge problems is became possible even on ordinary personal computers.

5. Implementation

An assembling and solution of FEM-matrices are performed using the FEniCS [9], PETSc and petsc4py packages [10]. For saving a memory and decreasing the assembling computation time the same fine mesh is used for all coarse subdomains which have the hexagonal or rectangular forms. The reinterpolation difficulty is vanished by the same positions of the nodal points on the opposite sides of the mesh. The matrices $\hat{L}$ and $\hat{R}$ are built in series by subdomins using the monolith format. The GMRES solver with Incomplete LU preconditioners are employed. The PCA analysis is performed by SciKit machine learning package [11].

III. NUMERICAL RESULTS

1. Problem definition

The RBE method is verified using a two-dimensional core steady-state problem which based on the well-known two-group pin-power benchmark NEACR-L336 [12]. The two types of fuel assemblies are employed: rodded/unrodded uranium and plutonium. Each assembly is represented by the 17×17 pin-level map of compositions which depicted in Fig.2. The two-group macro-cross sections are used. The checkerboard core with alternated uranium and plutonium assemblies is considered, Fig.3. There are 192 fuel assemblies in total. The aim is to simulate the steady-state power distributions for different positions of rodded assemblies using the same set of reduced basis functions.

2. Snapshots and reduced bases calculation

According to the considered core configuration the numerical model consists of the 256 subdomains which represented by the four types: unrodded uranium assembly (UX), rodded uranium assembly (UA), plutonium assembly (PX) and reflector (RR). Due to large distinctions in compositions the three sets of reduced bases are used: for uranium $U = \{UX, UA\}$, plutonium $P = \{PX\}$ and reflector $R = \{RR\}$ subdomains.

For the snapshots generation we need to determine the appropriate set of 2×2 patterns. Let us take the all combinations of fourth subdomains which to be found in the given core. We will take into account the presence of rodded and unrodded uranium assemblies as well. The total number of different patterns is 32, Fig.4. But because the rotation symmetry the actual number of patterns to be considered is 9 only.

For each considered pattern the reflection boundary conditions are imposed. During the steady-state power iterations the neutron flux distributions are accumulated within the errors from 10^{-2} to 10^{-6}. A fetched on given iteration distribution is defined overall on the pattern. Therefore it is split up to 4 parts and spread out the sets U, P or R. The total number of snapshots in each set is about 500.

Then reduced basis functions are generated by PCA analysis for each set of snapshots. The number of principal components is constrained by 100. The estimated variance rations of the components are depicted in Fig.5. According to this graphic the same number of basis functions is used in each of sets U, P or R.

3. Pin-by-pin calculations results

By the construction procedure the built reduced basis functions could be employed for a wide series of configurations including that depicted in Fig.3. An accuracy of the results is depend on a chosen dimension S_r of the reduced subspace. Let us estimate the most suitable number S_r^* by the comparison of RBE's results with reference solution.

The reference solutions of the considered steady-state problem obtained by the SKETCH-N code [13] using Polynomial Nodal Method (PNM). The k_{ef} and pin-level power distribution Fig.10 for configuration C calculated by PNM and RBE methods using a different number of employed reduced basis functions. Let us consider the behavior of errors of the RBE's results on dimension of reduced subspace S_r.

It is clear that increasing of dimension leads to decreasing of errors. As a rule there is a threshold S_r^* after that the further decreasing of errors is not significant and increasing of the dimension has not a big sense. The presence of the threshold in the RBE method is confirmed by the dependencies depicted in Fig.6 and Fig.7 where it could be seen that the number S_r^* equals 60.

The configurations A, B and C calculated by RBE method using the same number of basis functions. The errors of the results for all cases are stayed within $12pcm$ in k_{ef} and 1.5% in power distribution, I.

The maximum errors in power distributions are concentrated near the corners of assemblies, Fig.14.

There is a gain in the computation time of RBE method compared not only with the ordinary FEM but with the PNM method as well.

Unlike the nodal methods there is a large degree of freedom of the subdomains in RBE approach which leads to high computational costs on the assembling procedure. For example of considered two-dimensional problem it takes about 4 min of time and 1 GB of memory for the matrices $\hat{R}$ and $\hat{L}$. Therefore the preliminary approximation of the matrices entries is required when a problem with feedbacks is solved.

IV. CONCLUSIONS AND FUTURE DEVELOPMENTS

For the decreasing of computation costs the high-fidelity calculations could be provided by the construction of a proper reduced subspace and appropriate ROM. A reduced subspace is supplied by the analysis of the snapshots which are a set of solutions calculated by a high-fidelity model. If the dimension of the model is too large the generation of snapshots is become inadmissible expensive. In this case the spatial decomposition of the given problem will be useful.

The considered here RBE method is based on the PCA analysis of snapshots and generation of reduced bases on subdomains making up the reactor core. The DG method is employed to treat the discontinuities of the result solution appeared interfaces due to the different sets of basis functions on the adjacent fragments.

The actual boundary conditions at the assembly-wise fragments are unknown and too complicated for a low-order approximation. It prevents to calculate the suitable snapshots and prepare an appropriate basis functions. Therefore a new

approach have been developed where snapshots are fetched while a power iterations of the 2×2-patterns are performed. The numerical tests are confirmed the once generated by this way reduced bases could be applied for a wide set of core configurations.

In a real core configurations almost all assemblies are different and distinguished by a type of fuel, enrichment, burnup etc. Therefore a large number of bases sets for RBE method may be required, by own for each assembly. The suggested method of snapshots generation could be applied in this case by splitting the core on a set of overlapping 2×2 patterns. But the given configuration could not been changed without appropriate augmentation of the snapshots pull. Because a size of reduced matrices depend only on a number of subdomains and dimensions of truncated subspaces the number of reduced basis sets has not affect on the efficiency of the RBE method.

There are a few issues and tasks which should be solved before a practical implementation of the RBE method: adaptation to the three-dimensional multiphysics problems [5], [14], as example [15], development of the a-posteriori error estimation algorithm.

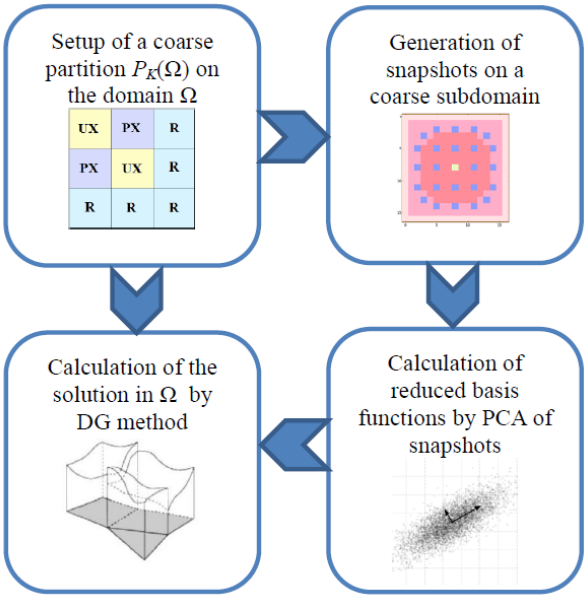

Fig. 1. The flowchart of the RBE method.

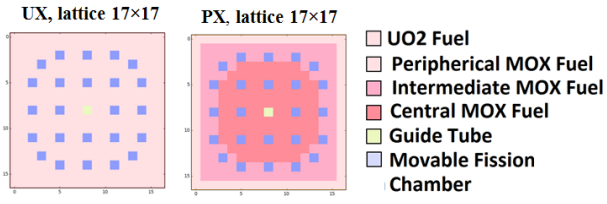

Fig. 2. The lattice configurations.

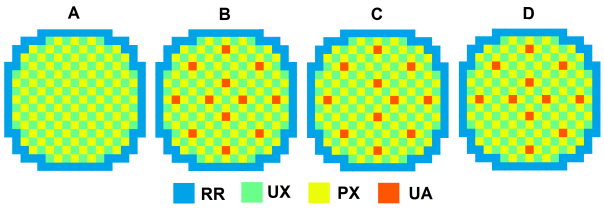

Fig. 3. The core configurations A, B and C.

```
1:  PX UX   UX PX
    UX PX   PX UX

2:  RR RR   RR RR   RR PX   RR RR
    RR PX   PX RR   RR RR   RR PX

3:  RR RR   RR RR   RR UX   RR RR
    RR UX   UX RR   RR RR   RR UX

4:  RR RR   RR PX   PX UX   UX RR
    UX PX   RR UX   RR RR   PX RR

5:  RR RR   RR UX   UX PX   PX RR
    PX UX   RR PX   RR RR   UX RR

6:  RR UX   PX UX   UX RR   UX PX
    UX PX   UX RR   PX UX   RR UX

7:  PX UA   UA PX
    UA PX   PX UA

8:  PX UX   UX PX
    UA PX   PX UA

9:  PX UA   UA PX
    UX PX   PX UX
```

Fig. 4. The 2×2 patterns for snapshot's calculations.

V. ACKNOWLEDGMENTS

We want to thank Andrey A. Semenov for an inspiration on this work and Richard Sanchez for useful discussions.

REFERENCES

1. G. ROZZA, D. HUYNH, and A. PATERA, "Reduced Basis approximation and A-Posteriori Error Estimation for Affinely Parametrized Elliptic Coercive Partial Differential Equations," *Archives of Computational Methods in Engineering*, **15**, 229–275 (2008).
2. A. QUARTIRONY, A. MANZONI, and F. NEGRI, *Reduced Basis Methods for Partial Differential Equations: An Introduction*, Springer (2016).
3. Y. LIANG, "Proper Orthogonal Decomposition and its Applications. Part I: Theory," *Journal of Sound and Vibration*, **252**, *3*, 527–544 (2002).
4. A. SEMENOV, N. SHCHUKIN, and N. RYABOV, "Using of the Reduction Order Model for the Reconstruction of the Power Distribution by the Lateral Ionization Chambers," *Journal of Nuclear Energy*, **4**, 47–54 (2007).
5. A. SARTORI, A. CAMMI, and L. LUZZI, "A Multi-Physics Reduced Order Model for the Analysis of the Lead Fast Reactor Single Channel," *Annals of Nuclear Energy*, **87**, 198–208 (2016).

Case	k-eff	$\Delta\rho$, pcm	Power error, % MAX	RMS	Calc. time, s RBE	PNM
A	1.015743	11	1.0	0.1	8	51
B	0.999149	13	1.0	0.1	13	54
C	1.003217	12	1.4	0.2	10	125
D	1.000999	12	1.3	0.2	18	206

TABLE I. Errors and performance of RBE method.

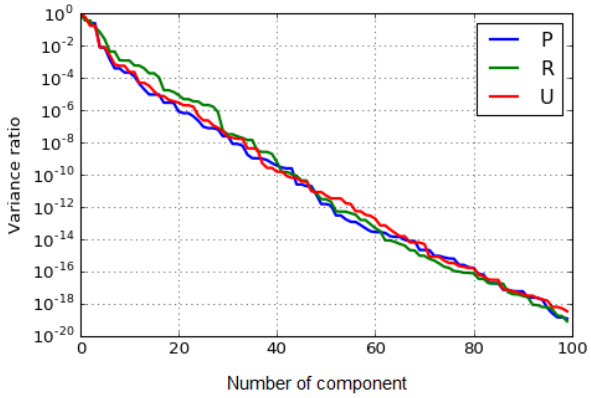

Fig. 5. The estimated variance rations on a number of principal component.

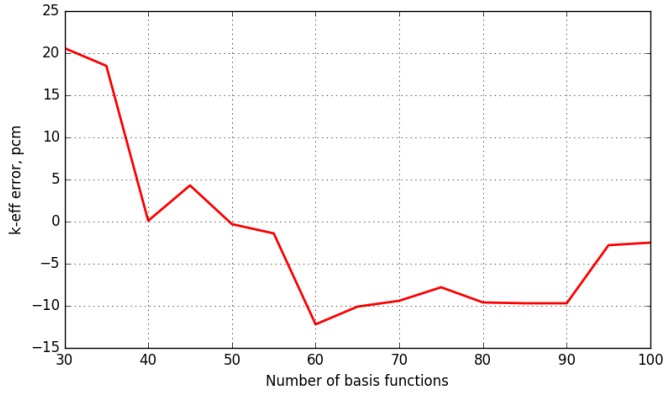

Fig. 6. The error of k_{ef} obtained by RBE method for configuration C.

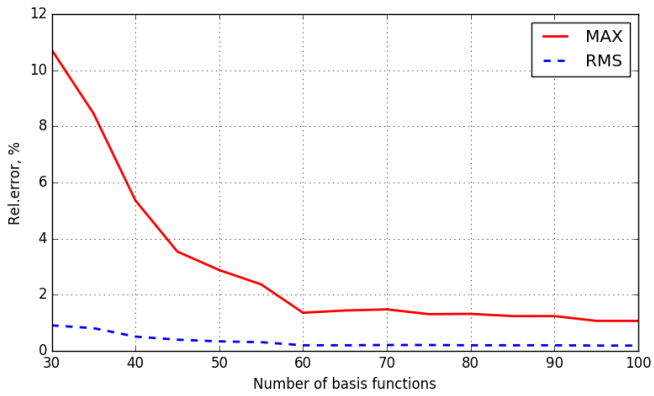

Fig. 7. A relative error of the power distribution obtained by the RBE method for the configuration C.

6. Y. MADAY and E. RONQUIST, "A Reduced-Basis Element Method," *Journal of Scientific Computing*, **17**, 1–208 (2002).
7. J. ODEN, I. BABUSKA, and C. BAUMANN, "A Discontinuous hp Finite Element Method for Diffusion Problems," *Journal of Computational Physics*, **146**, 491–519 (1998).
8. I. BABUSKA, C. BAUMANN, and J. ODEN, "A Discontinuous hp Finite Element Method for Diffusion Problems: 1-D Analysis," *Computers and Mathematics with Applications*, **37**, 103–122 (1999).
9. A. LOGG, K. MARDAL, and G. WELLS, *Automated Solution of Differential Equations by the Finite Element Method*, Springer. http://dx.doi.org/10.1007/ 978-3-642-23099-8 (2012).
10. S. BALAY, S. ABHYANKAR, M. F. ADAMS, J. BROWN, P. BRUNE, K. BUSCHELMAN, L. DALCIN, V. EIJKHOUT, W. D. GROPP, D. KAUSHIK, M. G. KNEPLEY, L. C. MCINNES, K. RUPP, B. F. SMITH, S. ZAMPINI, H. ZHANG, and H. ZHANG, "PETSc Users Manual," Tech. Rep. ANL-95/11 - Revision 3.7, Argonne National Laboratory (2016).
11. F. PEDREGOSA, G. VAROQUAUX, A. GRAMFORT, V. MICHEL, B. THIRION, O. GRISEL, M. BLONDEL, P. PRETTENHOFER, R. WEISS, V. DUBOURG, J. VANDERPLAS, A. PASSOS, D. COURNAPEAU, M. BRUCHER, M. PERROT, and E. DUCHESNAY, "Scikit-learn: Machine Learning in Python," *Journal of Machine Learning Research*, **12**, 2825–2830 (2011).
12. E. SATORI, "Final Specification of Benchmark NEACRP-L-336," Tech. Rep. NDB/91/1402/avt, OECD (1991).
13. V. ZIMIN, "SKETCH-N: A nodal neutron diffusion code for solving steady-state and kinetics problems, vol. 1. Model description," Tech. Rep. NEA-1577/01, JAERI (2000).
14. A. SARTORI, A. CAMMI, L. LUZZI, and G. ROZZA, "A Reduced Basis Approach for Modeling the Movement of Nuclear Reactor Control Rods," *Annals of Nuclear Energy*, **2**, *2* (2015).
15. E. RYU and H. JOO, "Finite Element Method Solution of the Simplified P3 Equations for General Geometry Applications," *Annals of Nuclear Energy*, **56**, 194–207 (2013).

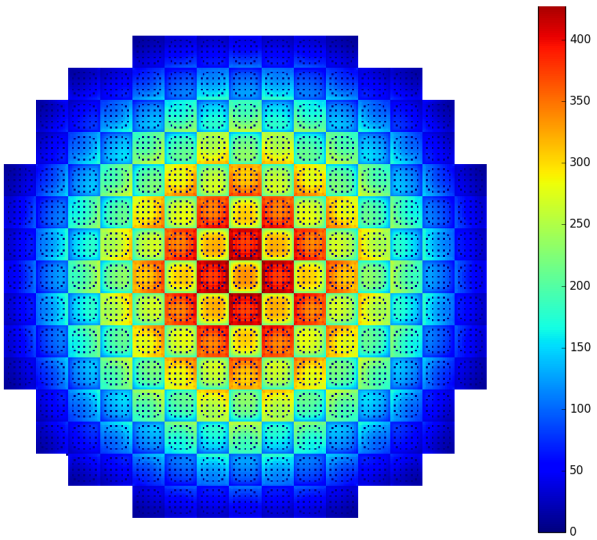

Fig. 8. The power distribution for the configuration A.

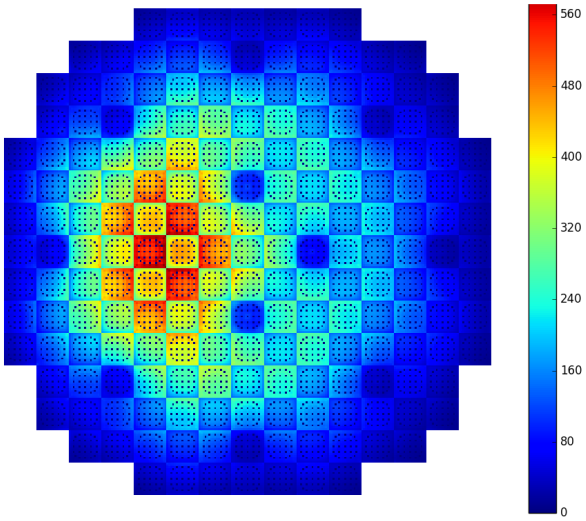

Fig. 10. The power distribution for the configuration C.

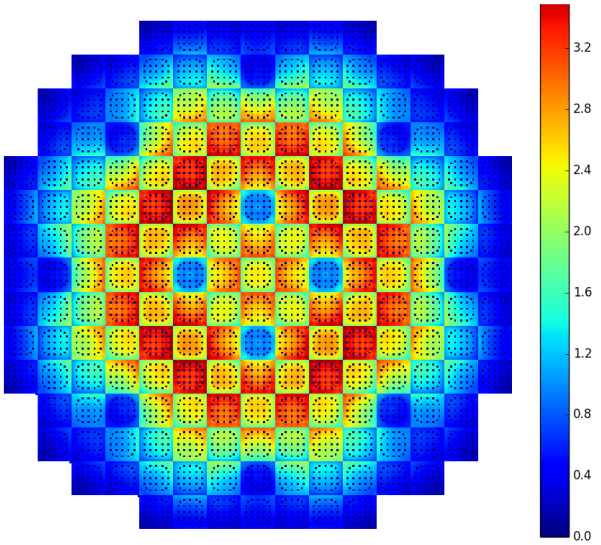

Fig. 9. The power distribution for the configuration B.

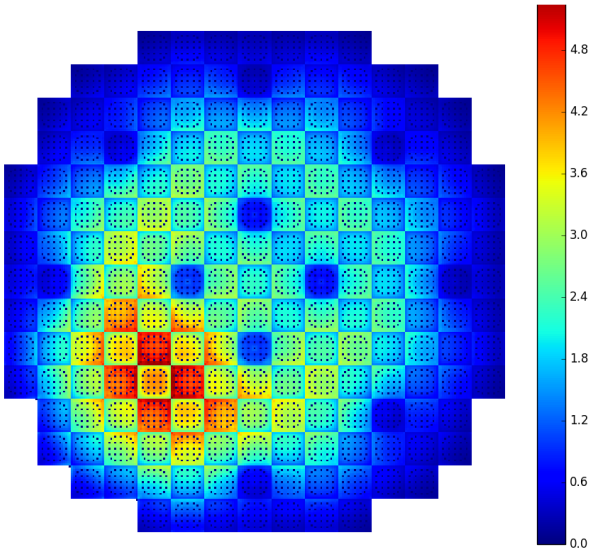

Fig. 11. The power distribution for the configuration D.

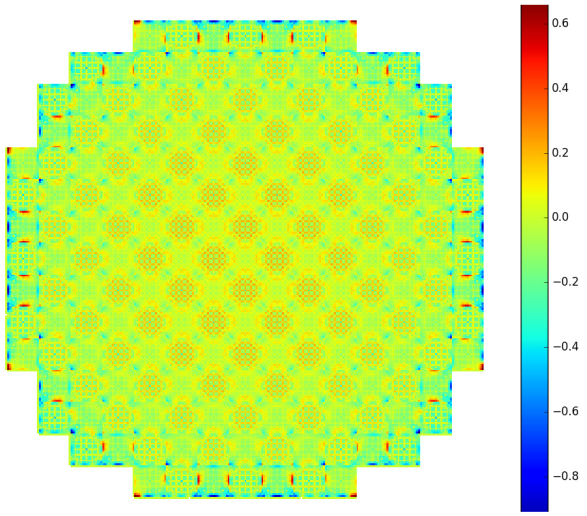

Fig. 12. The relative error of the power distribution for the configuration A.

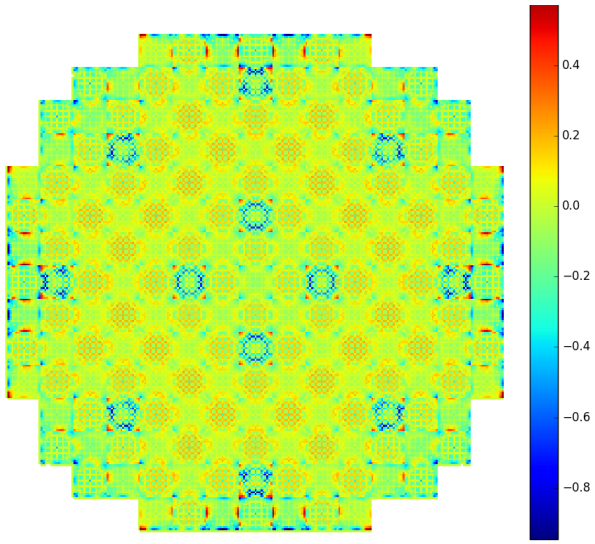

Fig. 13. The relative error of the power distribution for the configuration B.

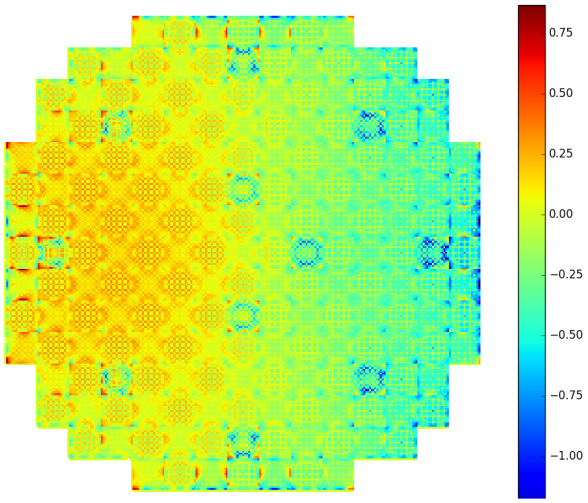

Fig. 14. The relative error of the power distribution for the configuration C.

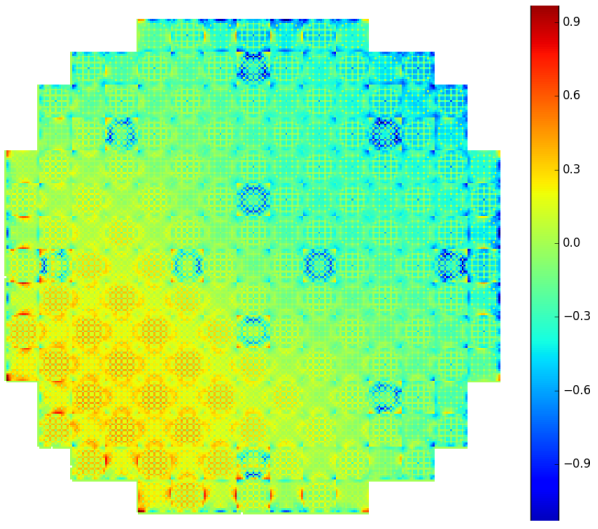

Fig. 15. The relative error of the power distribution for the configuration D.